

Magnetic ground states in the three Os⁶⁺ (5d²) double perovskites Ba₂MOsO₆ (M = Mg, Zn, and Cd) from Néel order to its suppression

C. A. Marjerrison,¹ C. M. Thompson,² A. Z. Sharma,³ A. M. Hallas,¹ M. N. Wilson,¹ T. J. S. Munsie,¹ R. Flacau,⁴ C. R. Wiebe,³ B. D. Gaulin,^{1,5,6} G. M. Luke,^{1,5,6} and J. E. Greedan^{2,5,*}

¹Department of Physics and Astronomy, McMaster University, Hamilton, Canada, L8S 4M1

²Department of Chemistry and Chemical Biology, McMaster University, Hamilton, Canada L8S 4M1

³Department of Chemistry, University of Winnipeg, Winnipeg, Canada, R3B 2E9

⁴Canadian Neutron Beam Centre, Canadian Nuclear Laboratory, Chalk River, Canada, K0J 1J0

⁵Brockhouse Institute for Materials Research, McMaster University, Hamilton, Canada, L8S 4M1

⁶Canadian Institute for Advanced Research, Toronto, Canada, M5G 1Z8

(Received 12 August 2016; published 27 October 2016)

Three closely related double perovskites (DP) based on the 5d² ion, Os⁶⁺, Ba₂MOsO₆, with M = Mg, Zn, and Cd have been prepared and characterized using x-ray (XRD) and neutron diffraction (ND), dc magnetization, heat capacity, and muon spin relaxation (μ SR) techniques. All three are cubic, *Fm-3m*, at ambient temperature from XRD with $\Delta d/d \sim 5 \times 10^{-4}$ resolution. For both M = Mg and Zn, ND data at 3.5 K and lower, $\Delta d/d = 2 \times 10^{-3}$, resolution show no signs of a distortion. The results are compared with the known DP material, Ba₂CaOsO₆, which shows antiferromagnetic (AF) order below $T_N = 49$ K and a moderate frustration index, $f \sim 4$, ($f = |\theta_{CW}|/T_N$), where θ_{CW} is the Curie-Weiss temperature. Ba₂MgOsO₆ with a unit cell constant $a_0 = 8.0757(1)$ Å, 3% smaller than for Ba₂CaOsO₆, also shows Néel order below $T_N = 51$ K with $f \sim 2$. However, Ba₂ZnOsO₆, $a_0 = 8.0975(1)$ Å, 0.27% larger than Ba₂MgOsO₆, does not show Néel order from either heat capacity or μ SR data. A zero field cooled/field cooled (ZFC/FC) irreversibility occurs near 30 K and a broad heat capacity anomaly is detected at a similar temperature. The μ SR data are consistent with a weak spin ordering with an onset below 28 K but with a coexisting dynamic component. Ba₂CdOsO₆ with $a_0 = 8.3190(1)$ Å, 0.5% smaller than Ba₂CaOsO₆, shows no evidence for any type of order/spin freezing to 0.47 K from any of the measurement techniques applied. The results for M = Zn and Cd appear to lie outside of the mean field theory of Chen and Balents [*Phys. Rev. B* **84**, 094420 (2011)] for cubic d² DP with strong spin orbit coupling, but Ba₂MgOsO₆, along with Ba₂CaOsO₆, is likely one of the three predicted AF phases. The remarkable contrast between the doppelgänger pairs M = Mg/Zn and M = Ca/Cd may be traceable to differences in electronic structure of the diamagnetic M ions. All of the super-super exchange pathways in these DP materials involve Os–O–M–O–Os linkages.

DOI: [10.1103/PhysRevB.94.134429](https://doi.org/10.1103/PhysRevB.94.134429)

I. INTRODUCTION

Interest in the B-site ordered double perovskites (DP) of composition A₂B¹B²O₆, has grown recently. If only the B¹ site is magnetic the potential for geometric magnetic frustration is present as the B¹ sublattice has a face centered topology, consisting of the edge-sharing tetrahedra, as shown in Fig. 1. In many cases, the B¹ ion is from the 4d or 5d transition metal series and phenomena, which are minor concerns with 3d elements, such as spin orbit coupling (SOC), acquire greater importance. Three series of these DP materials with B¹ electronic configurations $nd^1(t_{2g}^1)$, $nd^2(t_{2g}^2)$, and $nd^3(t_{2g}^3)$ have received the most attention. The t_{2g}^n notation comes from the octahedral site symmetry at the B¹ site in an ordered DP. Each series presents different issues. For example, t_{2g}^3 ions are orbital singlets, while the orbital moment is not fully quenched in the other two cases. As well, t_{2g}^1 and t_{2g}^2 ions are potentially subject to Jahn-Teller induced crystallographic distortions, while t_{2g}^3 ions are not. Several examples of DP based on t_{2g}^1 and t_{2g}^3 ions have been described recently. The t_{2g}^1 family exhibits a wide range of magnetic behaviors, ranging

from apparently simple Néel antiferromagnets (Ba₂LiOsO₆), ferromagnets (Ba₂MgReO₆ and Ba₂NaOsO₆), cooperative spin singlet ground states (Ba₂YMoO₆), and even spin glasses (Sr₂CaReO₆) [1–5]. On the other hand, the vast majority of t_{2g}^3 DP are uniformly AF showing Néel order, face-centered-cubic (fcc) type I, with wave vectors $\mathbf{k} = (000)$ or $(1/2 \ 1/2 \ 0)$, except for La₂NaRuO₆, which has incommensurate $\mathbf{k} = (000.091)$ order [6,7]. Interestingly, La₂NaOsO₆, Sr₂MgIrO₆, and Sr₂ZnIrO₆ do not order above 4 K [7,8].

Somewhat less is known about the t_{2g}^2 DP group of which there are about six examples that have been reasonably well characterized, as shown in Table I. Two ions are involved, Re⁵⁺ and Os⁶⁺, both 5d² and t_{2g}^2 in the DP B¹ site. Of this group, only Ba₂YReO₆ and SrLaMgReO₆ appear to be highly frustrated by the criterion of the frustration index [16]. Long range AF order has been demonstrated, convincingly, either via a heat capacity lambda peak and muon spin relaxation (μ SR) oscillations for Ba₂CaOsO₆ and heat capacity and neutron diffraction (ND) for Sr₂MgOsO₆. Ba₂YReO₆ and La₂LiReO₆ show complex spin freezing below the listed T_{ord} , and SrLaMgReO₆ does not order or undergo spin freezing above 2 K. Dominant AF spin correlations are observed for all DP, although competing F interactions cannot be ruled out. Interestingly, the mean field theory of Chen and Balents for

*Corresponding author: greedan@mcmaster.ca

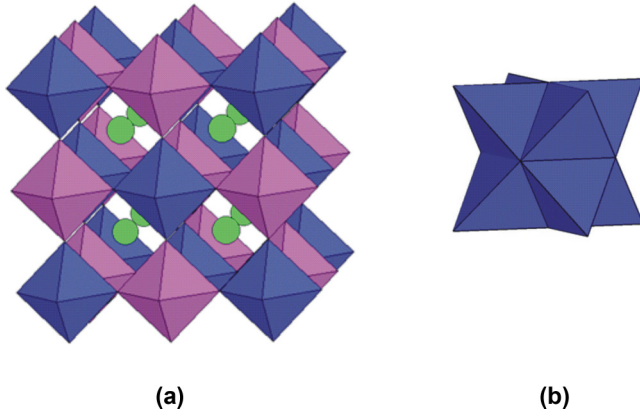


FIG. 1. (a) The structure of a cubic ($Fm\text{-}3m$) B -site ordered DP, $A_2BB'O_6$. The B and B' site octahedra are shown in magenta and blue, respectively, and the A cations are green. (b) Note that both the B and B' sites form a fcc lattice, the topology of which consists of the edge-sharing tetrahedra.

t_{2g}^2 ions subject to strong SOC in the cubic DP lattice predicts three F ground states, but none has ever been reported [17]. Ba_2YReO_6 and Ba_2CaOsO_6 are examples of what can be called the doppelgänger problem. The unit cell constants differ by only 0.01%, yet Ba_2CaOsO_6 is slightly frustrated, $f \sim 4$, while for Ba_2YReO_6 , $f \sim 18$. Also, Ba_2CaOsO_6 shows AF order below 49 K, while a complex spin freezing is seen in μ SR data for Ba_2YReO_6 . An ordered moment has been reported for only one AF t_{2g}^2 DP via ND, Sr_2MgOsO_6 with $\mu(Os^{6+}) = 0.60(2) \mu_B$ from powder data [14]. The ordered moment on Os^{6+} in Ba_2CaOsO_6 has been estimated as $\sim 0.2\text{--}0.3 \mu_B$ from analysis of μ SR internal fields [12].

The subjects of this paper are three t_{2g}^2 DP materials, namely, Ba_2MgOsO_6 , Ba_2ZnOsO_6 , and Ba_2CdOsO_6 . The computed Goldschmidt tolerance factors are 1.05, 1.04, and 0.993, respectively, and all are expected to be cubic, $Fm\text{-}3m$ [18]. As the radius of Cd^{2+} (0.95 Å) is very close to that for Ca^{2+} (1.00 Å), one might expect similar behavior for Ba_2CdOsO_6 and Ba_2CaOsO_6 . The radii of Mg^{2+} (0.72 Å) and Zn^{2+} (0.74 Å) are much smaller than Ca^{2+} but similar to each other, and comparisons should be revealing. Note also that the pairs Mg^{2+}/Zn^{2+} and Ca^{2+}/Cd^{2+} represent very different electronic configurations as Zn^{2+} and Cd^{2+} have filled nd shells, $3d^{10}$ and $4d^{10}$, respectively, while for Mg^{2+} and Ca^{2+} , $3d$ orbitals are empty. This may be important, as the principal super-super exchange pathways in DP involve the B ions, both

the nearest neighbor 90° and next nearest neighbor 180° cases, $Os\text{-}O\text{-}B\text{-}O\text{-}Os$. The three DP materials in this paper were reported in the 1960s, but only some synthetic details and low precision unit cell constants are available [19].

II. EXPERIMENTAL PROCEDURES

A. Synthesis

The Ba_2MOsO_6 ($M = Mg, Zn, \text{ and } Cd$) compounds were prepared by solid state reactions following, initially, literature synthetic procedures [19]. Common features of the preparation details were the use of $BaCO_3$, MO , and Os metal as starting materials. For $M = Zn$ and Cd , a 10% molar excess was necessary. In all cases, a 10% molar excess of Os metal was used. Reactions were carried out in air in a box furnace within a fume hood to avoid releasing toxic OsO_4 to the lab atmosphere. While the furnace temperature was always $1000^\circ C$, the optimum reaction times were determined by trial and error to be 96 h for $M = Mg$, 4 h for $M = Zn$ and 1 h for $M = Cd$. In the latter two cases, heating for longer times resulted in decomposition of the DP. Samples of composition Ba_2MWO_6 were also prepared to provide ‘‘lattice match’’ materials for the heat capacity measurements. These involved the starting materials $BaCO_3$, MO , and WO_3 and heating in air at $1200^\circ C$ for 48 h.

B. X-ray diffraction

The x-ray powder diffraction data were collected using a PANalytical X-Pert Pro diffractometer equipped with a linear X'Celerator detector and $CuK\alpha 1$ radiation ($\lambda = 1.54056 \text{ \AA}$) at ambient temperature for all samples over the range $10\text{--}120^\circ$ in 2θ , $Q_{\max} = 7.06 \text{ \AA}^{-1}$. Refinement of both x-ray and neutron powder diffraction data was accomplished using the FullProf suite of programs [20].

C. Neutron diffraction

Elastic neutron powder diffraction data for Ba_2MOsO_6 ($M = Mg$ and Zn) were collected at the Canadian Neutron Beam Centre, Chalk River Nuclear Laboratories, on the C2 diffractometer. A ~ 2 g sample was loaded into a vanadium can. Two incident wavelengths of neutrons were used, 1.33 and 2.37 Å. The wavelengths were calibrated against an Al_2O_3 standard. Measurements were performed at 3 and 290 K for each neutron wavelength. Temperature was controlled using a top-loading closed cycle refrigerator.

D. Magnetization

For Ba_2MOsO_6 (where $M = Mg, Zn, Cd$), zero field cooled (ZFC) and field cooled (FC) magnetic susceptibility measurements were performed using a superconducting quantum interference device (SQUID) magnetometer, Quantum Design Magnetic Property Measurement System, with an applied field of 0.05 T.

E. Heat capacity

Heat capacity measurements were performed using pellets of size 2–3 mg placed on a sapphire platform sample stage of a

TABLE I. Some magnetic and structural data for selected t_{2g}^2 DP.

DP	Space group	θ (K)	T_{ord} (K) ^a	f^b	Refs.
Ba_2YReO_6	$Fm\text{-}3m$	−616	35	~ 18	[9,10]
Ba_2CaOsO_6	$Fm\text{-}3m$	−156	49	~ 4	[11,12]
Sr_2MgOsO_6	$I4/m$	−347	108	~ 3	[13,14]
La_2LiReO_6	$P2_1/n$	−204	45	~ 4.5	[10]
$SrLaMgReO_6$	$P2_1/n$	−161	<2	>80	[15]
Ca_2MgOsO_6	$P2_1/n$	−72	19	~ 3.8	[13]

^aThis is either T_N or T_{sf} (spin freezing).

^b $f = |\theta_{\text{CW}}|/T_{\text{ord}}$, the frustration index [16].

DynaCool Physical Property Measurement System (Quantum Design) equipped with a helium three heat capacity insert puck. The pellets were adhered to the platform using Apiezon N Grease during the measurements. The measurements were performed in 0 and 9 T fields over a temperature range from 0.350 to 100 K. The heat capacity of the puck and grease were subtracted from the total heat capacity.

E. Muon spin relaxation

Zero field muon spin relaxation (ZF- μ SR) spectra were collected for Ba₂MOsO₆ ($M = \text{Mg, Zn, and Cd}$) on the M15 and M20 surface muon channels at TRIUMF National Laboratory in Vancouver, Canada. For Ba₂MgOsO₆ and Ba₂CdOsO₆, measurements were performed in the LAMPF time-differential spectrometer, which is equipped with a ⁴He cryostat, giving temperatures between 2 and 300 K. This apparatus provides an ultralow background such that only events originating from muons that land in the sample are recorded.

In a μ SR experiment, muons incident upon the sample penetrate several hundred micrometers, where they come to rest at a Coulomb potential minimum. The muon spin will then precess in the local magnetic environment. After an average lifetime of 2.2 μ s, the muon will decay, emitting a positron preferentially in the direction of the muon spin. These decay events are recorded by forward and backwards detectors, in front of and behind the sample. The time dependence of the positrons detected in the forward, N_F , and backward, N_B , detectors can be combined to give a muon decay asymmetry, defined as $A(t) = (N_F - N_B)/(N_F + N_B)$. The resulting asymmetry spectra were fitted using the μ SR fit software package [21].

III. RESULTS AND DISCUSSION

A. Structural studies: XRD and neutron powder diffraction

Crystal structures were refined in $Fm\bar{3}m$. The setting with Ba in $8c$ ($1/4\ 1/4\ 1/4$), B in $4b$ ($1/2\ 1/2\ 1/2$), Os in $4a$ ($0\ 0\ 0$), and O in $24e$ ($x\ 0\ 0$) was used. The x-ray data were taken at ambient temperature, 290 K, and neutron data at 290 and 3.5 K. Of course, for $B = \text{Cd}$, only x-ray data were obtained due to the large absorption cross section. The results of Rietveld refinements for all B are shown in Table II. In Figs. 2 and 3, the refinements are shown in detail for $B = \text{Zn}$. All others are available in the Supplemental Material [22].

The rather larger agreement index, χ^2 , for the $M = \text{Mg}$ ND data and problems with refinement of the displacement parameters, B , reflect the fact that the large (~ 3 g) sample used for these experiments was contaminated with $\sim 20\%$ of an impurity phase, Ba₁₁Os₄O₂₄, and some unreacted MgO. Details are given in the Supplemental Material [22]. The smaller sample used for the x-ray, magnetic susceptibility, heat capacity, and μ SR studies had minor levels, 2%, of the impurity phase. Nonetheless, it was still possible, via a multiphase refinement, to determine cell constants and oxygen positions to a reasonable degree of accuracy from the ND data. A problem was also encountered with the Os site for $M = \text{Zn}$ for both 290 and 3.5 K in the neutron data. The Os site displacement always refined to a small negative value and was thus fixed to a small positive value in the refinements. We argue that this does not imply significant B/B' site mixing as the displacements refine to positive definite values using the x-ray data, where the B/B' contrast is actually greater. Interatomic distances were calculated from the data in Table I and are given in the Supplemental Material [22]. The agreement with expected values is excellent.

TABLE II. Summary of Rietveld refinement results for Ba₂MOsO₆. $M = \text{Mg, Zn, and Cd}$.

290 K							
$M = \text{Mg}$							
	a_0 (Å)	x (O)	B (Å ²) [Ba]	B (Å ²) [Mg]	B (Å ²) [Os]	B (Å ²) [O]	χ^{2a}
X-ray	8.0757(2)	0.233(1)	1.45(7)	1.2(4)	1.31(6)	1.0(3)	1.98
Neutron	8.0734(9)	0.2402(3)	0.10	0.35(9)	0.10	0.20	4.24
$M = \text{Zn}$							
	a_0 (Å)	x (O)	B (Å ²) [Ba]	B (Å ²) [Mg]	B (Å ²) [Os]	B (Å ²) [O]	χ^{2a}
X-ray	8.0977(2)	0.238(1)	0.92(8)	0.7(1)	0.62(6)	0.9(2)	1.89
Neutron	8.0976(6)	0.2399(4)	0.39(4)	0.71(9)	0.10	0.7(1)	1.59
$M = \text{Cd}$							
	a_0 (Å)	x (O)	B (Å ²) [Ba]	B (Å ²) [Mg]	B (Å ²) [Os]	B (Å ²) [O]	χ^{2a}
X-ray	8.3190(1)	0.234(1)	0.69(4)	0.54(6)	0.29(4)	1.5(3)	1.24
3.5 K							
$M = \text{Mg}$							
	a_0 (Å)	x (O)	B (Å ²) [Ba]	B (Å ²) [Mg]	B (Å ²) [Os]	B (Å ²) [O]	χ^{2a}
Neutron	8.0549(4)	0.2396(3)	0.10	0.20	0.20	0.15(3)	13.0
$M = \text{Zn}$							
	a_0 (Å)	x (O)	B (Å ²) [Ba]	B (Å ²) [Mg]	B (Å ²) [Os]	B (Å ²) [O]	χ^{2a}
Neutron	8.0816(6)	0.2389(3)	0.05(4)	0.20(8)	0.14	0.34(3)	1.97

^a $\chi^2 = R_{\text{wp}}/R_{\text{exp}}$.

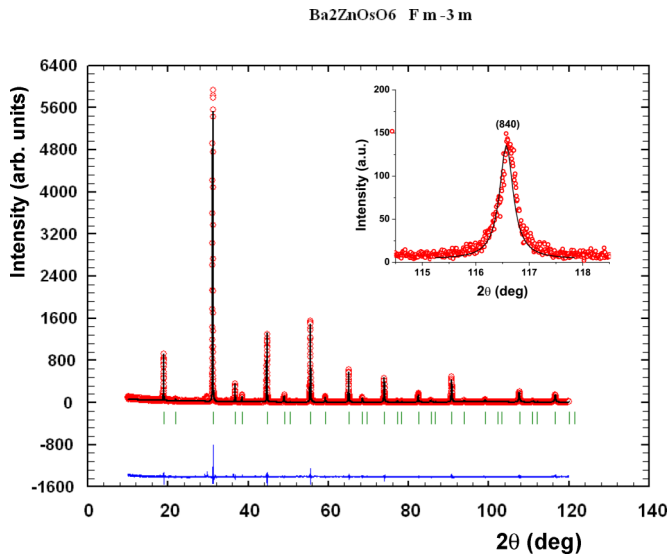


FIG. 2. Rietveld refinement of $\text{CuK}\alpha 1$ XRD data for $\text{Ba}_2\text{ZnOsO}_6$ at 280 K. Results are summarized in Table II. The (840) reflection fit to a single Lorentzian is shown in the inset. There is no discernable distortion away from $Fm\text{-}3m$ symmetry to within a resolution of $\Delta d/d = 5 \times 10^{-4}$.

Some results for $\text{Ba}_2\text{ZnOsO}_6$ are shown in Figs. 2 and 3. As Os^{6+} is a t_{2g}^2 ion, a Jahn-Teller distortion is a possibility. Thus, special care was taken to search for evidence for such a distortion. A Rietveld refinement of x-ray diffraction (XRD) data appears in Fig. 2.

The inset shows the (840) reflection with a fit to a single Lorentzian. These results indicate that the cubic $Fm\text{-}3m$ model fits the data very well at ambient temperature (280 K). The estimated resolution at the scattering angles of Fig. 2 is $\Delta d/d = 5 \times 10^{-4}$. In Fig. 3(a), the results of a Rietveld refinement of ND data are shown for the high bank detector position at 280 K. The fit to a very high angle reflection (862/10 2 0; inset) indicates the excellence of the $Fm\text{-}3m$ model. Finally, high angle data at 280 and 3.5 K are compared in Fig. 3(b), indicating no discernable change in symmetry upon cooling. The estimated resolution of the ND data in this angular range is $\Delta d/d = 2 \times 10^{-3}$.

To summarize, the structural results for all three samples, $M = \text{Mg}$, Zn , and Cd , both the x-ray, and neutron data are consistent with the $Fm\text{-}3m$ model both at 280 and 3.5 K (for $M = \text{Mg}$ and Zn) to within the resolution of the instruments used. In two cases, $M = \text{Mg}$ and Zn , an impurity phase, $\text{Ba}_{11}\text{Os}_4\text{O}_{24}$, was detected at the level of 2% by weight, but it was not detected in the $M = \text{Cd}$ sample. The presence of this phase has implications for the bulk magnetization studies, as described below.

The properties of the three materials, which include magnetization, heat capacity, and muon spin relaxation (μSR) are reported separately.

B. $\text{Ba}_2\text{MgOsO}_6$

1. Magnetization

Susceptibility data are shown in Fig. 4(a). Note the large anomaly beginning near 6 K. This is the signal from the

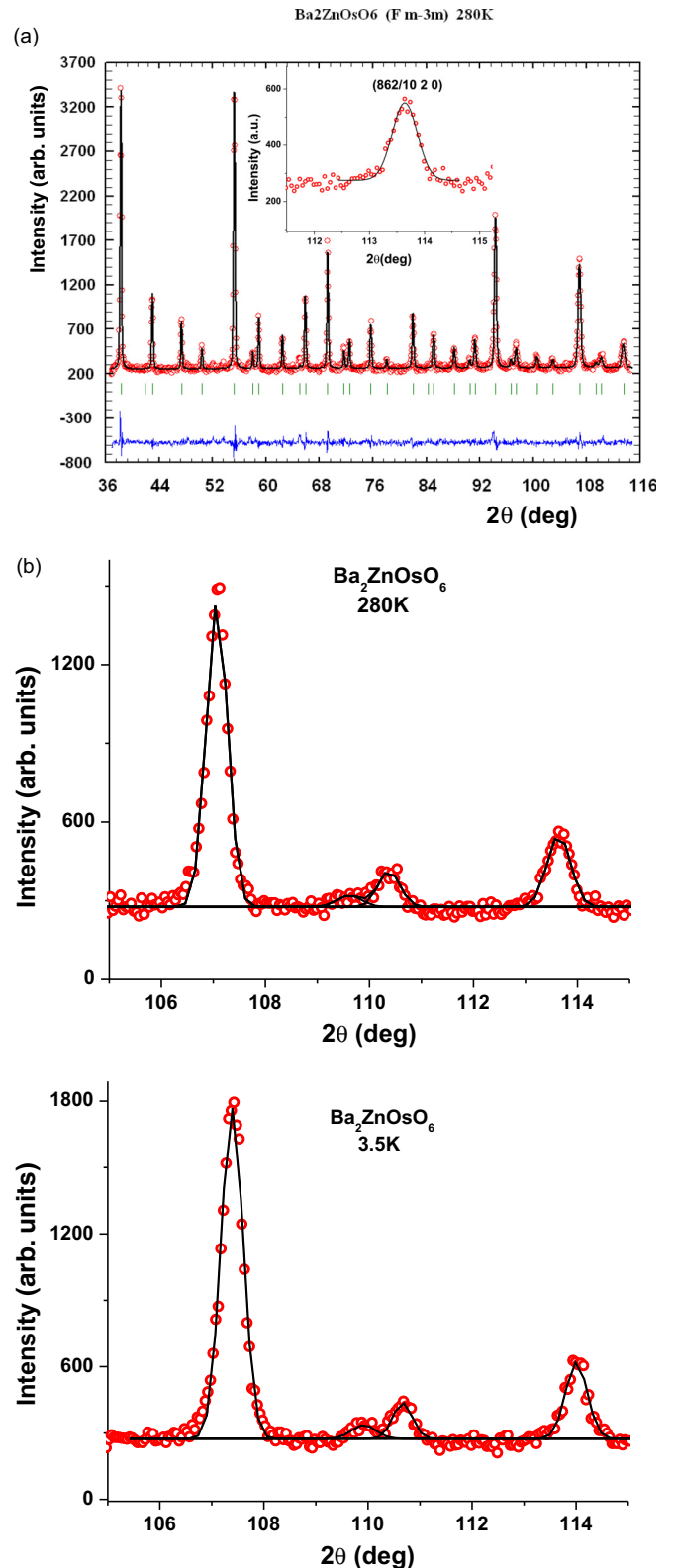


FIG. 3. (a) Rietveld fit to ND data (high bank setting) for $\text{Ba}_2\text{ZnOsO}_6$ at 280 K, $\lambda = 1.3280(1) \text{ \AA}$. The inset shows the fit to the (862/10 2 0) reflection. (b) Top: High angle ND data are for $\text{Ba}_2\text{ZnOsO}_6$ at 280 K. Bottom: Data are over the same range at 3.5 K. The red circles are the data; the black line is the fit to the $Fm\text{-}3m$ model. There is no discernable distortion from $Fm\text{-}3m$ symmetry upon cooling to a resolution of $\Delta d/d = 2 \times 10^{-3}$.

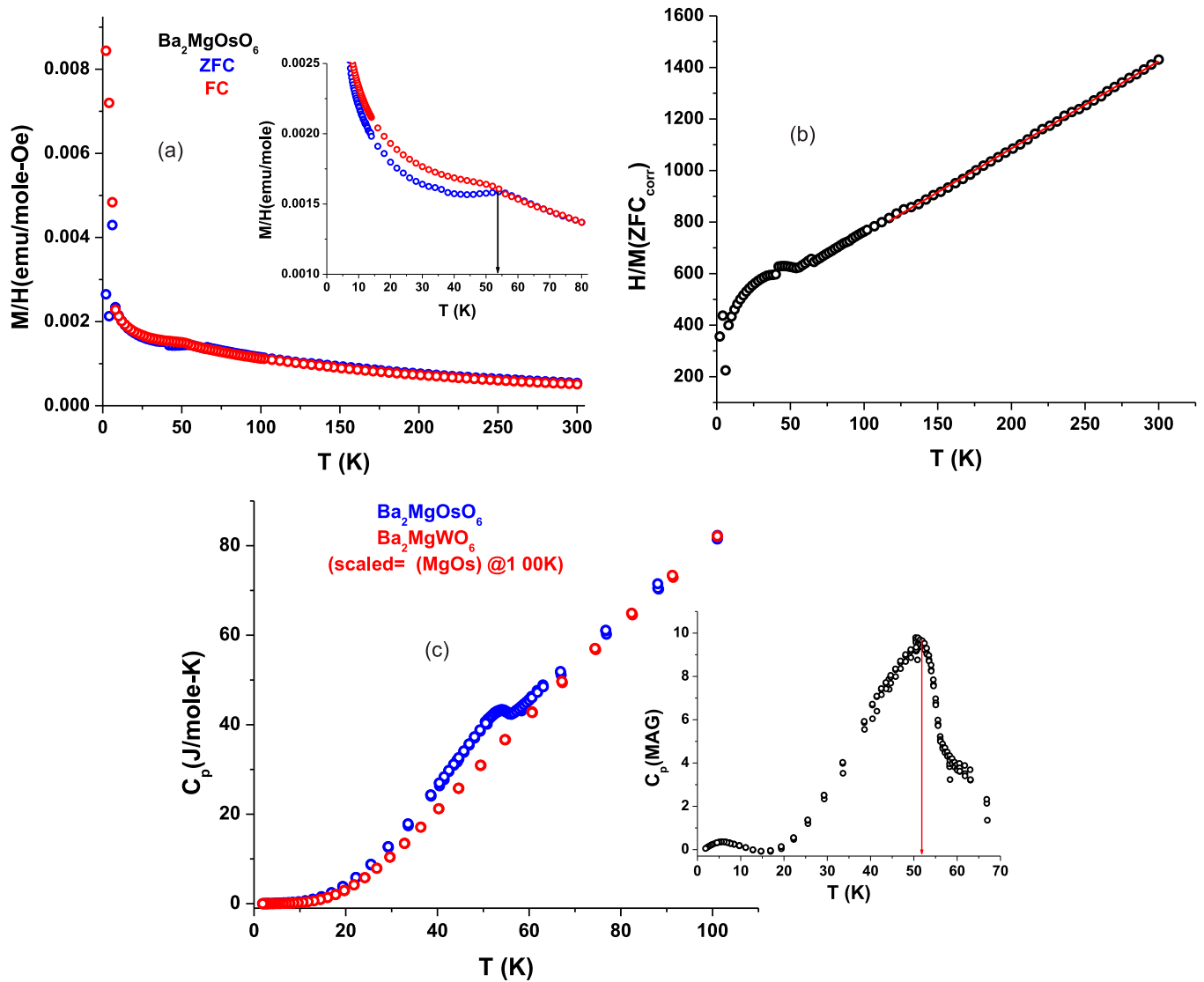


FIG. 4. (a) Magnetic susceptibility (H/M) for $\text{Ba}_2\text{MgOsO}_6$. The inset shows the region near 50 K. (b) Inverse susceptibility of $\text{Ba}_2\text{MgOsO}_6$, corrected for diamagnetism, showing adherence to the Curie-Weiss law over the range 125 to 300 K. The fitting parameters are $C = 0.295(1)$ emu/mole-K and $\theta_{\text{CW}} = -120(1)$ K. (c) Heat capacity data for $\text{Ba}_2\text{MgOsO}_6$ compared with scaled lattice match data (see text). The inset shows the estimated magnetic contribution. Note the clear peak centered at $T_N = 52$ K in both plots. The weak anomaly near 6 K is due to the impurity phase, $\text{Ba}_{11}\text{Os}_4\text{O}_{24}$.

impurity phase, $\text{Ba}_{11}\text{Os}_4\text{O}_{24}$, which is a weak ferromagnet with $T_N = 6$ K [23]. The inset focuses attention on the region near 50 K, where a ZFC/FC divergence is seen, suggesting that $\text{Ba}_2\text{MgOsO}_6$ undergoes a transition to an antiferromagnetic (AF) state below $T_N \sim 53$ K. As the molar susceptibilities of these DP materials are small, a diamagnetic correction, obtained from published tables, was applied to all of the data [24]. For $M = \text{Mg}$, $\chi_{\text{diam}} = -1.57 \times 10^{-4}$ emu/mole. The inverse susceptibility, H/M , displayed in Fig. 4(b), shows a good adherence to the Curie-Weiss law over the range 125–300 K. Analysis yields the parameters $C = 0.295(1)$ emu/mole-K ($\mu_{\text{eff}} = 1.536(2) \mu_B$), which can be compared with the spin only values of 1.00 emu/mole-K and $2.83 \mu_B$, respectively. Clearly, both are significantly reduced from the spin only values. The intercept, $\theta_{\text{CW}} = -120(1)$ K, is consistent with strong, net AF correlations. It is useful to compare these results

with those for $\text{Ba}_2\text{CaOsO}_6$, which are $C = 0.454$ emu/mole - K, $\mu_{\text{eff}} = 1.905 \mu_B$, $\theta_{\text{CW}} = -206(1)$ K, and $T_N = 49$ K. (Note: The CW parameters are different from the values reported in [12], as diamagnetic corrections had not been applied. The numbers quoted for that phase here result from analysis of corrected data.) In both cases, C and μ_{eff} are much reduced from the spin only values, but μ_{eff} for $M = \text{Mg}$ is significantly smaller than for $M = \text{Ca}$ and, as will be shown in the following sections, $M = \text{Zn}$ and Cd . The origin of this effect is not clear at present. Note also that while θ_{CW} for the $M = \text{Ca}$ phase is ~ 1.7 times that for $M = \text{Mg}$, T_N for the latter is about 6% higher than for $M = \text{Ca}$, which is consistent with its smaller unit cell constant.

Finally, note that there was no evidence in the ND data at 3.5 K for any magnetic reflections, parallel to the case for $M = \text{Ca}$ reported earlier [12]. Thus, it is important to confirm

the presence of a phase transition in this material by other measurements, such as heat capacity and μ SR.

2. Heat Capacity

Heat capacity data compared to scaled lattice (Ba_2MgWO_6) data are shown in Fig. 4(c). The lattice match was not ideal as the data exceeded those for $\text{Ba}_2\text{MgOsO}_6$ above ~ 70 K. Thus, a scale factor was applied to the data for Ba_2MgWO_6 such that the two heat capacities were equal at 100 K. The inset shows an estimate of the magnetic contribution obtained by subtraction of the scaled lattice component. Note that in both cases a clear peak is seen near 52 K, corroborating the T_N deduced from the magnetization data. In the magnetic contribution a very weak feature is seen near 6 K, due the $\text{Ba}_{11}\text{Os}_4\text{O}_{24}$ impurity phase. Given the quantitative uncertainties associated with the lattice contribution, no further analysis was deemed warranted.

C. Muon spin relaxation

The zero field muon decay asymmetry spectra for $\text{Ba}_2\text{MgOsO}_6$ are shown in Fig. 5(a) at a selection of temperatures. Below $T_N = 52$ K, there is an oscillatory component to the asymmetry, which is a hallmark of static magnetic order on the muon timescale. The solid lines are the fits to the data given by (1), where the three components have asymmetries of A_1 , A_2 , and A_3 , which are constrained to be temperature independent. This fitting function contains a strongly relaxing component (λ_1), to capture the early time asymmetry, a slowly relaxing component (λ_2) to capture the long-time asymmetry, and an oscillating (cosine) component, with a frequency of ω/γ_μ , where ω is the size of the internal field and γ_μ is the muon gyromagnetic ratio. Muons will come to rest in the most electronegative positions, which in the present materials will be near the oxygen ions. The number of symmetrically inequivalent oxygen sites then determines the number of muon stopping sites, which is one in the $Fm-3m$ structural model

consistent with the single oscillating component in the fitting function. The temperature dependence of the internal field size gives an order parameter, as shown in Fig. 5(b) with $T_N = 52$ K, in agreement with the magnetization and heat capacity data. At low temperatures, the magnitude of the internal field reaches its maximum value, 62(1) G. This is the same value as previously found in $\text{Ba}_2\text{CaOsO}_6$, indicating that the ordered Os^{6+} moment is in the range 0.2–0.3 μ_B [12].

$$A(t) = A_1 \exp(-\lambda_1 t) + A_2 \exp(-\lambda_2 t) + A_3 \cos(\omega t / \gamma_\mu) \times \exp(-\lambda_3 t). \quad (1)$$

In summary, $\text{Ba}_2\text{MgOsO}_6$ shows weak frustration, $f = 2$, and clearly orders into an AF ground state below 52 K. It is very similar to isostructural $\text{Ba}_2\text{CaOsO}_6$, $f = 4$ and $T_N = 49$ K. The small increase in T_N vis à vis the $M = \text{Ca}$ phase can be understood in terms of the 3% smaller unit cell constant that would enhance the strength of the super-super exchange interactions. The magnetic structure is unknown for either case and the very small internal fields, ~ 60 G, extracted from analysis of the μ SR data, are essentially identical, and point to a very small ordered moment on Os^{6+} in the range 0.2 to 0.3 μ_B .

D. $\text{Ba}_2\text{ZnOsO}_6$

There are even stronger similarities between the $M = \text{Mg}$ and $M = \text{Zn}$ DP, as the unit cell constants now differ by only 0.3%, due to the similar ionic radii of Mg^{2+} and Zn^{2+} . However, the electronic structures of the M^{2+} ions are quite different and the M^{2+} ions are involved, as has been pointed out, in the super-super exchange pathways present in these cubic DP oxides.

1. Magnetization

These data are displayed in Figs. 6(a) and 6(b). The data shown in Fig. 6(b) were corrected for a diamagnetic

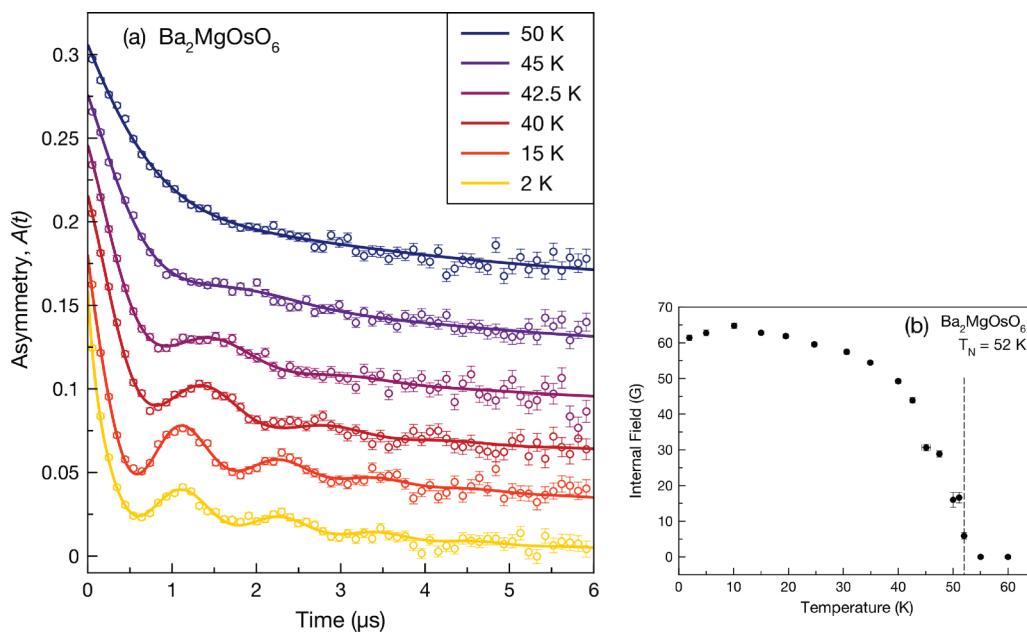


FIG. 5. (a) Zero-field μ SR data at several temperatures. The solid lines are fits to (1) (see text). (b) Temperature dependence of the internal field seen by the muon, consistent with $T_N = 52$ K.

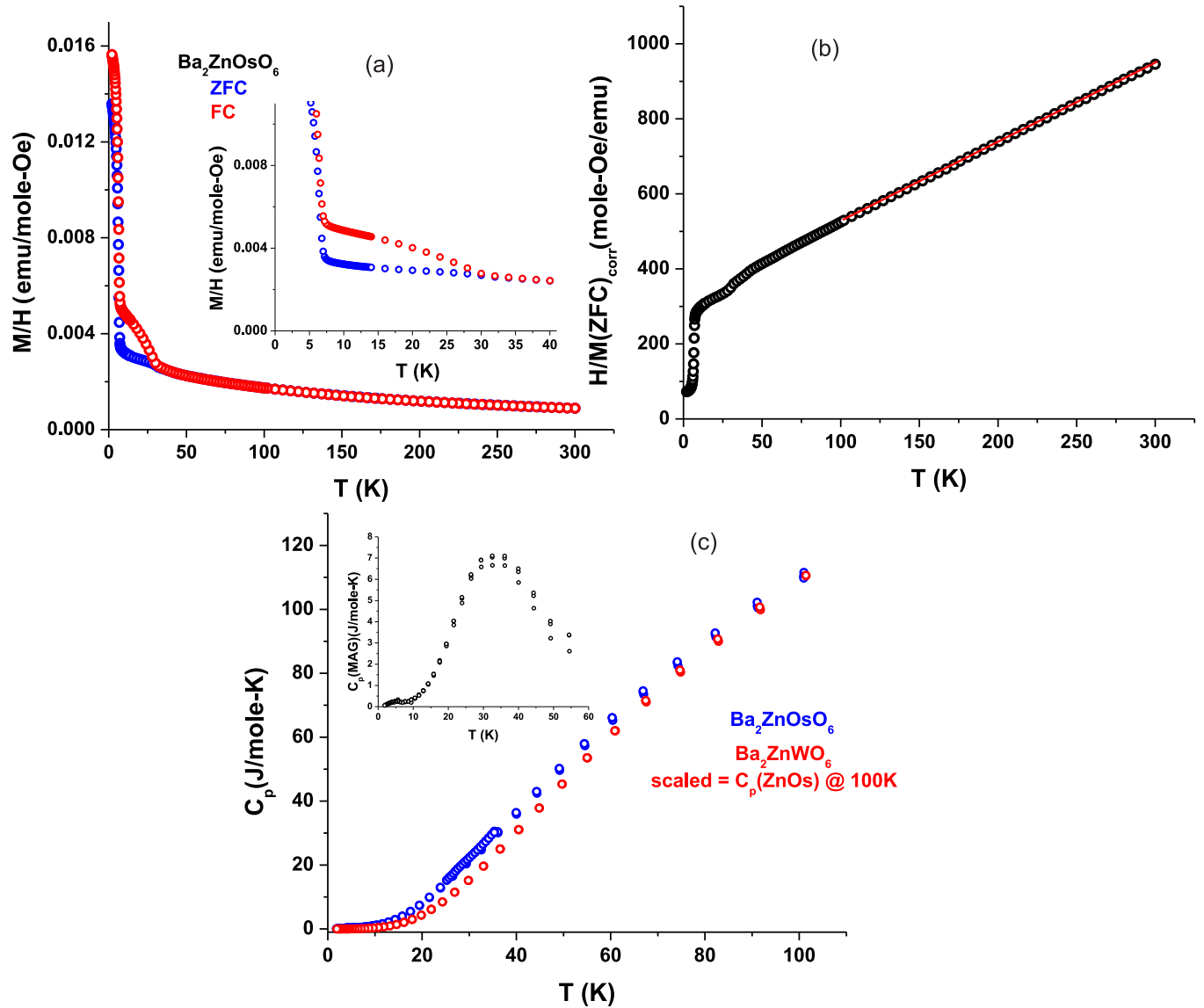


FIG. 6. (a) Magnetic susceptibility for $\text{Ba}_2\text{ZnOsO}_6$. Note the ZFC/FC anomaly near 30 K. The data below 6 K are dominated by the impurity phase, $\text{Ba}_{11}\text{Os}_4\text{O}_{24}$. (b) Inverse susceptibility data for $\text{Ba}_2\text{ZnOsO}_6$ (corrected for diamagnetism) showing excellent adherence to the Curie-Weiss law. The derived parameters are $C = 0.4737(6)$ emu/mole-K and $\theta_{\text{CW}} = -149.0(4)$ K. (c) Heat capacity data at zero applied field for $\text{Ba}_2\text{ZnOsO}_6$. Note the absence of any sharp feature near the 30 K magnetic anomaly. The estimated magnetic contribution, inset, does show a broad maximum centered slightly above 30 K.

contribution, $\chi_{\text{diam}} = -1.64 \times 10^{-4}$ emu/mole. As in the case of $M = \text{Mg}$, the low temperature data are dominated by the impurity phase, $\text{Ba}_{11}\text{Os}_4\text{O}_{24}$, but there is a clear ZFC/FC divergence near 30 K, as seen most obviously in the inset to Fig. 6(a). Also, as for $M = \text{Mg}$, the inverse susceptibility data, Fig. 6(b), are well described by the Curie-Weiss law over a wide range, ~ 100 to 300 K. The derived parameters are $C = 0.4737(6)$ emu/mole-K [$\mu_{\text{eff}} = 1.947(2) \mu_{\text{B}}$], well below the spin only values of 1.00 emu/mole-K [$2.83 \mu_{\text{B}}$]; $\theta_{\text{CW}} = -149.4(4)$ K, somewhat larger than for $M = \text{Mg}$. Taking the ~ 30 K anomaly as a transition to some type of ordered or quasiordered state, $f = 5$. The nature of the 30 K anomaly is not clear from the magnetization data alone, and heat capacity and μSR studies were also undertaken.

2. Heat capacity

The heat capacity data for $\text{Ba}_2\text{ZnOsO}_6$ appear in Fig. 6(c). Again, it was necessary to scale the lattice match data to equal that for $\text{Ba}_2\text{ZnOsO}_6$ at 100 K. Immediately evident is the absence of any obvious anomaly near the 30 K magnetic feature. This is in sharp contrast to the situation for $M = \text{Mg}$. The estimated magnetic contribution, inset, does show a very broad maximum centered somewhat above 30 K. This strongly indicates that the apparent 30 K phase transition does not lead to a long range ordered AF ground state.

3. Muon spin relaxation

In Fig. 7(a), a selection of the zero field μSR asymmetry for $\text{Ba}_2\text{ZnOsO}_6$ between 2 and 40 K are plotted. Below 28 K, an

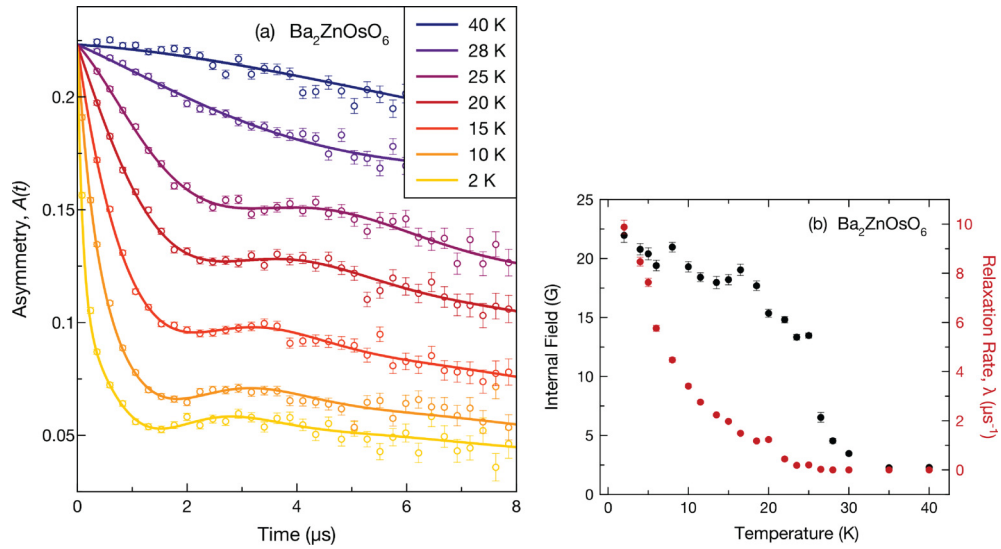


FIG. 7. (a) Temperature evolution of the asymmetry parameter for $\text{Ba}_2\text{ZnOsO}_6$. Note the onset of a rapid decrease just below 30 K and the development of a weak oscillatory component.(see text for discussion). (b) The temperature dependence of the internal field due to the oscillatory component (black circles) and the early time relaxation rate (red circles).

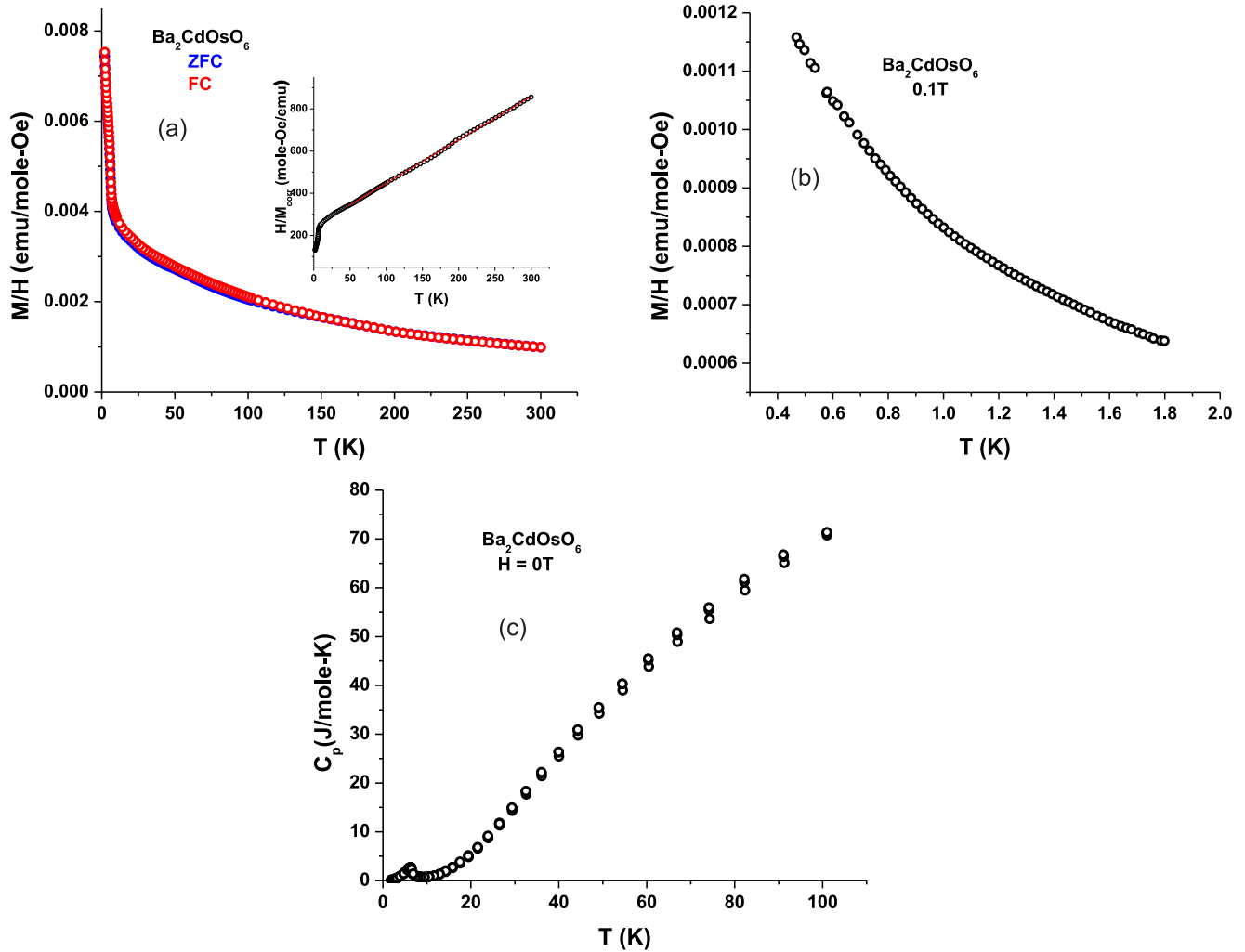


FIG. 8. (a) Magnetic susceptibility data for $\text{Ba}_2\text{CdOsO}_6$. Note the absence of any anomaly or ZFC/FC divergence above 6 K. The inset shows the inverse susceptibility and the adherence to the Curie-Weiss law over a wide temperature range.(b) Magnetic susceptibility from 1.8 to 0.47 K showing no evidence for a phase transition.(c) Heat capacity data showing no anomaly except that due to the $\text{Ba}_{11}\text{Os}_4\text{O}_{24}$ impurity phase near 6 K.

oscillatory component to the asymmetry spectra develops. The total asymmetry spectra are fit by the same function (1), shown by the solid lines, used above for Ba₂MgOsO₆. Thus, as above, there is only a single oscillation frequency corresponding to a single muon stopping site. The magnitude of the internal field at the lowest temperatures in Ba₂ZnOsO₆ is only 20 G, a factor three smaller than in Ba₂MgOsO₆. Furthermore, the oscillating signal accounts for only 15% of the total asymmetry, as compared to 27% in Ba₂MgOsO₆. This may suggest a partially ordered magnetic state at low temperature. The full temperature dependence of the fitted value of the internal field is plotted in Fig. 7(b). This forms an order parameter of sorts, correlated with approximately 30 K. Concomitant with the development of oscillations, there is a sharp increase in the early time relaxation rate, also shown in Fig. 7(b). This early time relaxation is not easily decoupled by application of a longitudinal field up to 1 kG, indicating that the state at 2 K remains at least partially dynamic. Thus, Ba₂ZnOsO₆ shows an ordered component below 28 K coexisting with a component showing persistent spin dynamics to 2 K. This is in sharp contrast to Ba₂MgOsO₆ that finds an AF ground state below 52 K. This is very surprising as the $M = \text{Zn}$ and $M = \text{Mg}$ DP oxides differ by less than 0.3% in unit cell constant. These facts indicate that the diamagnetic M element plays an unexpectedly important role in the determination of the magnetic ground state of these materials.

E. Ba₂CdOsO₆

This DP oxide has a unit cell constant intermediate between those for $M = \text{Mg}$ and Zn and $M = \text{Ca}$, but is much closer to the latter, being smaller by only 0.5%. Recall that the $M = \text{Ca}$ phase shows AF order below 49 K [11,12].

1. Magnetization

Susceptibility data, Fig. 8, show no sign of an anomaly or ZFC/FC divergence above 6 K, where the impurity phase signal occurs. The observation of the impurity phase for this sample is somewhat surprising, as no second phase was evident in the XRD. The inset displays the inverse susceptibility, corrected for a diamagnetic contribution, $\chi_{\text{diam}} = -1.76 \times 10^{-4}$ emu/mole, which again obeys the Curie-Weiss law over a very wide temperature range, ~ 50 to 300 K. The derived parameters are $C = 0.486(1)$ emu/mole-K [$\mu_{\text{eff}} = 1.972(2)\mu_{\text{B}}$] and $\theta_{\text{CW}} = -117.7(6)$ K, values quite similar to those for $M = \text{Zn}$. Data were also obtained within the temperature range 0.4 to 1.8 K, Fig. 8(b). Within this range the component from the impurity phase will be saturated and temperature independent; thus, any temperature dependent signal is due to Ba₂CdOsO₆. Note the absence of any indication of a phase transition to 0.47 K.

2. Heat Capacity

These results are displayed in Fig. 8(c). In this case the lattice match data proved to be unsuitable as the heat capacity of Ba₂CdWO₆ exceeded that for the Os phase already at 15 K, so no attempt was made to isolate a “magnetic” component. Note the absence of any anomaly within the measured range except that due to the impurity phase at 6 K.

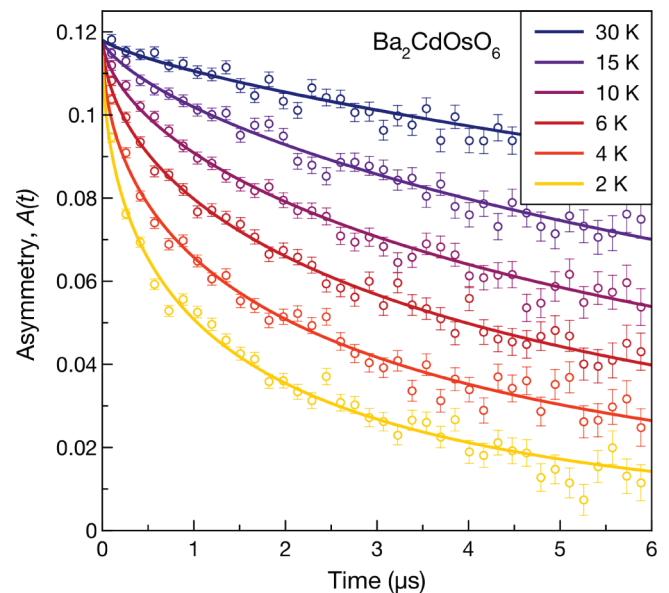


FIG. 9. Zero field μSR data for Ba₂CdOsO₆, showing only a gradual relaxation with decreasing temperature and no sign of either long range order or spin freezing.

3. Muon spin relaxation

In Fig. 9, the zero field μSR asymmetry for Ba₂CdOsO₆ are plotted between 2 and 30 K. The fits to the data, indicated by the solid lines, are stretched exponential functions given by (2), which well describe the data over the full temperature range measured. Down to 2 K, there is no sign of oscillatory behavior, which would signal long-range order, or a line shape, such as Kubo-Toyabe, or a more complex shape that would be consistent with spin freezing [25,26]. There is a gradual onset of relaxation, which might indicate the approach to a transition at lower temperatures. However, the susceptibility data of Fig. 8(b) suggests that such a temperature would be lower than 0.47 K

$$A(t) = A_1 \exp(-\lambda t)^\beta. \quad (2)$$

IV. SUMMARY AND CONCLUSIONS

Three closely related DP oxides based on the $5d^2$ ion Os⁶⁺, Ba₂MOsO₆, $M = \text{Mg}$, Zn , and Cd , have been synthesized and characterized with respect to crystal structure and a variety of physical probes, including dc magnetization, heat capacity, and μSR with the goal of determining the nature of the magnetic ground state. To within the resolution of the x-ray and neutron powder diffraction data, two, $M = \text{Mg}$ and Zn , are well described by the $Fm-3m$ structural model both at ambient temperature and 3.5 K. No low temperature data are available for the $M = \text{Cd}$ phase, but it is clearly $Fm-3m$ at ambient temperature. Ba₂MgOsO₆ shows Néel order below $T_N = 52$ K and is very similar to the known DP, Ba₂CaOsO₆, with $T_N = 49$ K. Both DP show moderate frustration indices, in the range $f = 2$ to 4. The magnetic structure of neither is known, but the ordered moment on Os⁶⁺ is likely of the order 0.2 to 0.3 μ_{B} . Note that the mean field theory of Chen and Balents for cubic $5d^2$ DP predicts three ordered AF or

Néel ground states, but lacking information about the magnetic structure, no assignment can be made [17].

Taking these four Os⁶⁺ DP as a related group, one can identify what might be called doppelgänger pairs, namely, $M = \text{Mg}/\text{Zn}$ and Ca/Cd , as the unit cell constants differ by no more than 0.5% within each pair. Yet, remarkably, while Ba₂MgOsO₆ has an AF ground state below 52 K, Ba₂ZnOsO₆ enters a complex partially ordered, partially dynamic state below 30 K, and Ba₂CdOsO₆ does not order in any sense to 0.47 K. That is, the Néel ground state can be significantly modified or even destroyed by the apparently benign chemical substitutions indicated. Presumably, this can be traced to differences in electronic structure between the doppelgänger pairs as all of the super-super exchange pathways in DP oxides involve Os–O–M–O–Os linkages. Computational studies are clearly needed as is further work to investigate the possibility

of local magnetic correlations in the $M = \text{Zn}$ and Cd phases. Determination of the magnetic structures of the $M = \text{Ca}$ and Mg DP oxides should also be an important goal.

ACKNOWLEDGMENTS

J.E.G., G.M.L., C.R.W., and B.D.G. thank the Natural Sciences and Engineering Research Council of Canada for support via the Discovery Grant Program. C.R.W. also acknowledges support from the Canadian Foundation for Innovation and the Canada Research Chair program, Tier II. P. Dube assisted with collection of magnetization and heat capacity data. We thank the TRIUMF Centre for Molecular and Materials Science (CMMS) staff for invaluable assistance with the muon spin relaxation experiments.

-
- [1] K. E. Stitzer, M. D. Smith, and H.-C. zur Loye, *Solid State Sci.* **4**, 311 (2002).
- [2] T. Aharen, J. E. Greedan, C. A. Bridges, A. A. Aczel, J. Rodriguez, G. MacDougall, G. M. Luke, T. Imai, V. K. Michaelis, S. Kroecker, H. Zhou, C. R. Wiebe, and L. M. D. Cranswick, *Phys. Rev. B* **81**, 224409 (2010).
- [3] M. A. de Vries, A. C. McLaughlin, and J.-W. G. Bos, *Phys. Rev. Lett.* **104**, 177202 (2010).
- [4] J. P. Carlo, J. P. Clancy, T. Aharen, Z. Yamani, J. P. C. Ruff, J. J. Wagman, G. J. Van Gastel, H. M. L. Noad, G. E. Granroth, J. E. Greedan, H. A. Dabkowska, and B. D. Gaulin, *Phys. Rev. B* **84**, 100404(R) (2011).
- [5] C. R. Wiebe, J. E. Greedan, G. M. Luke, and J. S. Gardner, *Phys. Rev. B* **65**, 144413 (2002).
- [6] C. M. Thompson, C. A. Marjerrison, A. Z. Sharma, C. R. Wiebe, D. D. Maharaj, G. Sala, R. Flacau, A. M. Hallas, Y. Cai, B. D. Gaulin, G. M. Luke, and J. E. Greedan, *Phys. Rev. B* **93**, 014431 (2016).
- [7] A. A. Aczel, D. E. Bugaris, L. Li, J.-Q. Yan, C. de la Cruz, H.-C. zur Loye, and S. E. Nagler, *Phys. Rev. B* **87**, 014435 (2013).
- [8] P. Kayser, M. J. Martinez-Lopez, J. A. Alonso, M. Retuerto, M. Croft, A. Ignatov, and M. T. Fernandez-Diaz, *Inorg. Chem.* **52**, 11013 (2013).
- [9] Y. Sasaki, Y. Doi, and Y. Hinatsu, *J. Mater. Chem.* **12**, 2361 (2002).
- [10] T. Aharen, J. E. Greedan, C. A. Bridges, A. A. Aczel, J. Rodriguez, G. MacDougall, G. M. Luke, V. K. Michaelis, S. Kroecker, C. R. Wiebe, H. Zhou, and L. M. D. Cranswick, *Phys. Rev. B* **81**, 064436 (2010).
- [11] K. Yamamura, M. Wakeshima, and Y. Hinatsu, *J. Solid State Chem.* **179**, 605 (2006).
- [12] C. M. Thompson, J. P. Carlo, R. Flacau, T. Aharen, I. A. Leahy, J. R. Pollicemi, T. J. S. Munsie, J. Munevar, T. Medina, S. Cheung, T. Goko, Y. J. Uemura, G. M. Luke, and J. E. Greedan, *J. Phys.: Condens. Matter* **26**, 306003 (2014).
- [13] Y. Yaun, H. L. Feng, M. P. Ghimine, Y. Matsushita, Y. Tsujimoto, J. He, M. Tanaka, Y. Katsuya, and K. Yamaura, *Inorg. Chem.* **54**, 3422 (2015).
- [14] R. Morrow, A. E. Taylor, D. J. Singh, J. Xiong, S. Rodan, U. B. Wolter, S. Wurmehl, B. Büchner, M. B. Stone, A. I. Kolesnikov, A. A. Aczel, A. D. Christianson, and P. M. Woodward, *Sci. Rep.*, **6**, 32462 (2016).
- [15] C. M. Thompson, L. Chi, J. R. Hayes, A. M. Hallas, M. Wilson, I. P. Swainson, A. P. Grosvenor, G. M. Luke, and J. E. Greedan, *Dalton Trans.* **44**, 10806 (2015).
- [16] A. P. Ramirez, *Annu. Rev. Mater. Sci.* **24**, 453 (1994).
- [17] G. Chen and L. Balents, *Phys. Rev. B* **84**, 094420 (2011).
- [18] V. M. Goldschmidt, *Naturwissenschaften* **14**, 477 (1926).
- [19] A. W. Sleight, J. Longo, and R. Ward, *Inorg. Chem.* **1**, 245 (1962).
- [20] J. Rodríguez-Carvajal, *Phys. B (Amsterdam, Neth.)* **192**, 55 (1993).
- [21] A. Suter and B. M. Wojek, *Phys. Procedia* **30**, 69 (2012).
- [22] See Supplemental Material at <http://link.aps.org/supplemental/10.1103/PhysRevB.94.134429> for Rietveld refinements of both x-ray and neutron powder data for Ba₂MgOsO₆ and of x-ray powder data for Ba₂CdOsO₆. Selected interatomic distances for all three compounds are also listed.
- [23] M. Wakeshima and Y. Hinatsu, *Solid State Commun.* **136**, 499 (2005).
- [24] P. W. Selwood, *Magnetochemistry* (Interscience Publishers, New York, 1956).
- [25] R. Kubo and T. Toyabe, in *Magnetic Resonance and Relaxation*, edited by R. Blinc (North Holland, Amsterdam, The Netherlands 1967), p. 810.
- [26] Y. J. Uemura, T. Yamazaki, D. R. Harshman, M. Senba, and E. J. Ansaldo, *Phys. Rev. B* **31**, 546 (1985).